



Research Paper

Cholesterol enrichment in liver mitochondria impairs oxidative phosphorylation and disrupts the assembly of respiratory supercomplexes



Estel Solsona-Vilarrasa^{a,b,c,d,1}, Raquel Fucho^{a,b,c,1}, Sandra Torres^{a,b,c}, Susana Nuñez^c,
 Natalia Nuño-Lámbarri^{a,b,f}, Carlos Enrich^{b,d}, Carmen García-Ruiz^{a,b,c,e,*},
 José C. Fernández-Checa^{a,b,c,e,*}

^a Department of Cell Death and Proliferation, Institute of Biomedical Research of Barcelona (IIBB), CSIC, Barcelona, Spain

^b Liver Unit, Hospital Clinic I Provincial de Barcelona, Instituto de Investigaciones Biomédicas August Pi i Sunyer (IDIBAPS), Barcelona, Spain

^c Centro de Investigación Biomédica en Red (CIBEREHD), Barcelona, Spain

^d Department of Biomedical Sciences, Medicine Faculty, Universitat de Barcelona (UB), Spain

^e Research Center for ALPD, Keck School of Medicine, University of Southern California, Los Angeles, CA, United States

^f Translational Research Unit, Medica Sur Clinic & Foundation, Mexico City, Mexico

ARTICLE INFO

Keywords:

Mitochondria
 Cholesterol
 Liver
 Hepatic diseases
 Respiration
 Oxidative stress

ABSTRACT

Mitochondrial cholesterol accumulation is a hallmark of alcoholic and non-alcoholic fatty liver diseases and impairs the function of specific solute carriers through changes in membrane physical properties. However, its impact on mitochondrial respiration and organization of respiratory supercomplexes has not been determined so far. Here we fed mice a cholesterol-enriched diet (HC) supplemented with sodium cholate to examine the effect of cholesterol in mitochondrial function. HC feeding increased liver cholesterol content, which downregulated *Srebp2* and *Hmgcr* expression, while sodium cholate administration decreased *Cyp7a1* and *Cyp8b1* mRNA levels, suggesting the downregulation of bile acid synthesis through the classical pathway. HC-fed mice exhibited increased expression of *Stard1* and *Mln64* and enhanced mitochondrial free cholesterol levels (2–3 fold), leading to decreased membrane fluidity. Mitochondria from HC-fed mice displayed increased cholesterol loading in both outer and inner mitochondrial membranes. Cholesterol loading decreased complex I and complex II-driven state 3 respiration and mitochondrial membrane potential. Decreased respiratory and uncoupling control ratio from complex I was also observed after *in situ* enrichment of mouse liver mitochondria with cholesterol or enantiomer cholesterol, the mirror image of natural cholesterol. Moreover, *in vivo* cholesterol loading decreased the level of complex III₂ and the assembly of respiratory supercomplexes I₁ + III₂ + IV and I₁ + III₂. Moreover, HC feeding caused oxidative stress and mitochondrial GSH (mGSH) depletion, which translated in hepatic steatosis and liver injury, effects that were rescued by replenishing mGSH with GSH ethyl ester. Overall, mitochondrial cholesterol accumulation disrupts mitochondrial functional performance and the organization of respiratory supercomplexes assembly, which can contribute to oxidative stress and liver injury.

1. Introduction

Cholesterol is an integral component of cellular membranes that not only plays an essential role in determining membrane physical properties, but also regulates multiple signaling pathways [1–3]. Due to this key role in modulating membrane structure and function, cholesterol levels in cell membranes are tightly regulated. Cells satisfy their need

for cholesterol either through the uptake from nutrients and cholesterol-rich low-density lipoproteins, or by *de novo* synthesis from acetyl-CoA in the mevalonate pathway controlled by HMG-CoA reductase (HMGCR), the rate-limiting step in cholesterol synthesis. The endoplasmic reticulum (ER)-based transcription factor SREBP-2 is a master regulator of cholesterol synthesis by controlling the expression of HMGCR [3,4].

Abbreviations: ALD, Alcoholic Liver Disease; DHE, Dihydroethidium; FFA, Free Fatty Acids; HC, High-Cholesterol diet; HMGCoA R, HydroxyMethylGlutaryl CoA Reductase; StARD1, Steroidogenic Acute Regulatory protein; TMRM, Tetramethylrhodamine Methyl ester; HPLC, High-Performance Liquid Chromatography; PMH, primary mouse hepatocytes

* Corresponding authors. Department of Cell Death and Proliferation, Institute of Biomedical Research of Barcelona (IIBB), CSIC, Barcelona, Spain.

E-mail addresses: cgrbam@iibb.csic.es (C. García-Ruiz), checa229@yahoo.com (J.C. Fernández-Checa).

¹ Both authors contributed equally to the work.

<https://doi.org/10.1016/j.redox.2019.101214>

Received 11 February 2019; Received in revised form 24 April 2019; Accepted 6 May 2019

Available online 09 May 2019

2213-2317/ © 2019 The Authors. Published by Elsevier B.V. This is an open access article under the CC BY-NC-ND license (<http://creativecommons.org/licenses/by-nc-nd/4.0/>).

Cholesterol is distributed from the plasma membrane and ER to different membrane bilayers, including mitochondria, where it plays key functional and structural roles. Mitochondria are essential organelles with numerous functions in cellular metabolism and homeostasis. They have long been considered as crucial organelles acting as the source of energy in the form of ATP synthesis. Besides this key function, mitochondria are also crucial for other cellular processes, including autophagy, apoptosis, fatty acid synthesis, Ca^{2+} homeostasis and cell signaling [5]. In addition, mitochondrial function extends beyond the boundaries of the cell and influence the physiology of the organism by regulating communication between cells and tissues [6]. Given this plethora of functions, it is not surprising that mitochondrial dysfunction has emerged as a key factor in a myriad of diseases [7–10]. Furthermore, mitochondria are the main consumers of molecular oxygen in the cell in the respiratory chain, which can result in the collateral generation of reactive oxygen species (ROS) [11–13].

Mitochondria are cholesterol-poor organelles compared to plasma membranes. The levels of cholesterol in mitochondrial membranes are under tight control, particularly in specialized organs, such as steroidogenic tissues or liver, where mitochondrial cholesterol is metabolized into steroid hormones or bile acids, respectively. The rate-limiting step in this metabolic process is determined by the cholesterol availability in mitochondria and therefore its mitochondrial trafficking regulates mitochondrial cholesterol homeostasis under physiological conditions. Mitochondrial cholesterol trafficking is controlled largely by STAR family members, including STARD1 and MLN64 (also known as STARD3) [14–16], and the unbalance between cholesterol trafficking and its metabolism can result in mitochondrial cholesterol accumulation, which can impact mitochondrial membrane physical properties and fluidity [17]. Indeed, mitochondrial cholesterol loading has been shown to perturb the function of specific membrane carriers, such as SLC25A11, which results in mitochondrial GSH (mGSH) depletion through impaired transport of cytosolic GSH into mitochondria, leading to increased oxidative stress [18–20].

Mitochondrial cholesterol accumulation is a hallmark of chronic diseases, including cardiovascular disorders, cancer and Alzheimer's disease [21–28]. In addition, previous studies have shown an association between increased mitochondrial cholesterol levels and liver injury in alcoholic and nonalcoholic liver disease [29–34]. However, the specific role of mitochondrial cholesterol accumulation in mitochondrial respiration and organization of functional respiratory complexes has not been previously examined. Therefore, our aim was to use *in vivo* and *in vitro* models of mitochondrial cholesterol enrichment to examine the impact of this event on oxygen consumption rates and the assembly of mitochondrial respiratory supercomplexes.

2. Material and methods

2.1. Animals and treatments

Wild type C57BL/6J male mice were obtained from Charles River Laboratories. All procedures involving animals and their care were approved by the Ethics Committee of the University of Barcelona and were conducted in accordance with institutional guidelines in compliance with national and international laws and policies. Mice were randomly separated in two groups that were fed with a regular chow diet (CTRL) or a high cholesterol diet (HC, 2% cholesterol and 0.5% sodium cholate, custom made Research Diets, Brogaarden Denmark, C18021901) for up to two days, as described previously [19]. In some cases, mice were fed with a diet enriched in 0.5% sodium cholate (SC) (Research Diet) alone. To test the role of mGSH replenishment, mice were fed HC diet and treated with 1.25 mmol/kg of GSH ethyl ester (GSH_{ee}), as described previously [35].

2.2. Mitochondria isolation and ROS determination

Livers were minced in 10 vol of cold Buffer A (225 mM mannitol, 75 mM sucrose, 0.1 mM EGTA, 10 mM HEPES and 1 mg/ml fatty acid-free BSA, pH 7.4) supplemented with protease and phosphatase inhibitors (Roche). Tissue was then disrupted with a drill-driven Teflon dounce homogenizer (4 strokes at 1500 rpm). Mitochondria were isolated by differential centrifugation, 15 min at $700 \times g$ followed by 15 min at $10000 \times g$ at 4 °C. Pellets containing mitochondria were resuspended in Buffer B (395 mM sucrose, 0.1 mM EGTA and 10 mM HEPES, pH 7.4).

ROS generation was determined in isolated mitochondria using MitoSox and Amplex Red Hydrogen peroxide/Peroxidase Assay Kit under basal conditions as described previously [36] and detailed in Supplemental Materials.

2.3. Mitoplasts preparation

Mitoplasts were prepared by permeabilization of intact mitochondria by digitonin. Briefly, to a mitochondrial protein suspension of 8 $\mu\text{g}/\mu\text{l}$ in Buffer B (395 mM sucrose, 0.1 mM EGTA and 10 mM HEPES, pH 7.4) an equal volume of digitonin (7.68 $\mu\text{g}/\mu\text{l}$) was added (960 μg digitonin/mg mitochondria). After incubation for 30 min at 4 °C, the sample was centrifuged for 10 min at $10000 \times g$ at 4 °C, and the pellet was resuspended in Buffer B and centrifuged again for washing. Mitoplasts purity was assessed by the presence of Porin or COX IV.

2.4. *In vitro* cholesterol increase in mouse liver mitochondria

In vitro cholesterol enrichment was performed by incubation of mitochondria with a cholesterol-BSA Complex (CBSAC) or enantiomer cholesterol (Ent-CBSAC) as described previously [32]. Enantiomer cholesterol was described before and generously provided by Scott Rychnovsky (Department of Chemistry, University of California Irvine) [37]. CBSAC and Ent-CBSAC were prepared by dissolving 50 mg of cholesterol or enantiomer cholesterol in 5 ml of absolute ethanol and then diluted with 5 ml of double distilled water. The milk-like solution was then centrifuged at $2000 \times g$ for 10 min. The supernatant was discarded, and the pellet was resuspended in 5 ml of Buffer CHS (0.25 M sucrose, 1 mM EDTA, pH 7.3). The white solution was stirred gently and 2 g of Free-Fatty Acid BSA were slowly added at room temperature. Once BSA was completely dissolved, the pH of the solution was adjusted to 7.3, and then centrifuged in the cold at $12000 \times g$ for 10 min. The supernatant was collected and used for cholesterol incorporation into mitochondria. CBSAC or ent-CBSAC was added to mouse liver mitochondria (0.2 mg/mg mitochondria) at 4 °C for 1 min. Mitochondria were subsequently diluted about 20 times with cold Buffer CHS, and spun down immediately at $12000 \times g$ for 10 min to eliminate the unbound cholesterol. Parallel control experiments were performed using only BSA.

2.5. Electron microscopy

Mice were perfused through the portal vein to wash the liver with cold saline and then fixed by perfusion with 2.5% glutaraldehyde in phosphate buffer. Liver tissue fragments were extracted and fixed with glutaraldehyde 2.5% and paraformaldehyde 2% in buffer phosphate (0.1 M, pH 7.4), post-fixed in 1% osmium tetroxide and 0.8% potassium ferrocyanide, dehydrated with acetone, and embedded in epoxy resin. Sections were cut and stained with methylene blue for light microscopy. Ultrathin sections for transmission electron microscopy were cut and stained with 2% uranyl acetate for 10 min and with a lead-staining solution for 2 min. Images from stained ultrathin sections were acquired by moving randomly across the EM grid using a transmission electron microscope JEOL JEM-1010 fitted with a Gatan Orius SC1000 (model 832) digital camera. ImageJ software was used to quantify the number

and length of mitochondria.

2.6. Measurement of fluorescence anisotropy

Fluidity of mitochondrial membranes was evaluated by fluorescence anisotropy of mitochondria-bound dye DPH. DPH (20 mM in tetrahydrofuran) was first diluted 100 times with 10 mM Tris-HCl, 150 mM KCl, 1 mM EDTA, pH 7.4. Subsequently, DPH was injected into stirred mitochondrial suspensions (0.5 mg/ml) and the mixture was incubated for 30 min at 37 °C. Fluorescence polarization was measured in a Hitachi spectrofluorometer at wavelengths of 366 nm for excitation and 425 nm for emission. The results are expressed as anisotropy units (r), where $r = (I_0/I_{90})/(I_0 + 2I_{90})$. I_0 and I_{90} represent the intensities of light when polarizers were in parallel or perpendicular orientation, respectively. Light scattering and intrinsic fluorescence were routinely corrected by subtracting the signal obtained from unlabeled samples and the fluorescence of the buffer plus label alone.

2.7. Blue-Native PAGE

Blue-Native PAGE was performed as described previously [38,39]. Briefly, 200 µg of mitochondria were isolated and solubilized using solubilization buffer A (50 mM Sodium Chloride, 50 mM Imidazole, 2 mM 6-aminohexanoic acid, EDTA 1 mM, pH 7) with digitonin (6 mg digitonin/mg mitochondria). Mitochondrial complexes were subsequently separated using a Criterion™ TGX™ Precast 4–15% gel (Biorad) and Running Buffer 10x Tris/Gly (Biorad), and transferred to a PVDF membrane using the Trans Blot Turbo (Biorad). To detect OXPHOS (super)complexes, the membrane was incubated overnight with the following primary antibodies: COXIV (Cell Signaling, #4844), UQCRC2 (G-10) (Santa Cruz, sc-390378) and MitoProfile® Total OXPHOS Rodent WB Antibody Cocktail (Abcam, ab110413). Membranes were thoroughly washed with TBS-Tween and incubated for 45 min with HRP-conjugated secondary antibody. Pierce ECL Western Blotting Substrate (ThermoScientific) was used to develop the membranes. Images were digitally captured by LAS4000 (GE Healthcare) and optical density was analyzed with ImageJ software. Coomassie blue staining was used as loading control.

2.8. Real time PCR

Total RNA was isolated from mouse liver with Trizol reagent (ThermoScientific) and converted to cDNA using the High-Capacity cDNA Reverse Transcription Kit from ThermoFisher. Quantitative Reverse Transcription Polymerase Chain Reaction (qRT-PCR) was subsequently performed using the SensiFAST™ SYBR® No-ROX Kit (Bioline) following the manufacturer's instructions. Each reaction was run in triplicate to determine the threshold (CT) for each mRNA, and the amount of each cDNA relative to the β2-Microglobulin (B2M) endogenous control was determined using the 2-ΔΔCt method. The primer sequences (Invitrogen) for the expression of *Sreb2*, *Hmgcr*, *Stard1*, *Mln64*, *Cyp27a1*, *Cyp7a1*, *Cyp7b1*, *Cyp8b1* and *B2M* are described in [Supplementary Table 1](#).

2.9. Extracellular flux analyses

0.2 µg protein/µl mitochondria stocks were prepared in cold MAS buffer (70 mM sucrose, 220 mM mannitol, 10 mM KH₂PO₄, 5 mM MgCl₂, 2 mM HEPES, 1.0 mM EGTA and 0.2% (w/v) fatty acid-free BSA, pH 7.2) with pyruvate and malate (10 mM) or succinate (10 mM) and rotenone (2 µM) as substrates for respiration. 50 µl of mitochondrial suspension (10 µg) were delivered per well of XFe24 Seahorse plate and plates were spun 15 min at 2000 × g at 4 °C. After centrifugation, 450 µl of warm (37 °C) MAS buffer with substrates were added. Plates were incubated 8–10 min at 37 °C in an incubator without CO₂ to allow the plate to warm and then loaded into the XFe24 Analyzer for

mitochondrial respiration analysis. Mitochondria began in a coupled state with substrate present; pyruvate and malate (10 mM) or succinate (10 mM) and rotenone (2 µM) (state 2). State 3 was initiated with ADP (4 mM) addition, state 4 was induced with the injection of oligomycin (2.5 µg/ml) (state 4o), and FCCP (4 µM) induced maximal uncoupler-stimulated respiration (state 3u). Non-mitochondrial respiration was assessed by OCR measurement in the presence of antimycin (4 µM). All states were sequentially measured, allowing calculation of respiratory control ratios (RCR: state 3/state 4o, or UCR: state 3u/state 4o). 3–5 mitochondrial preparations per experimental group were analyzed always in triplicates in each plate. Measurement protocol for standard liver mitochondria: 2 cycles of 1 min mix and 3 min measure per state. Measurement protocol for liver mitochondria after incubation with CBSAC: 2 cycles of 1 min mix and 4 min measure (State 2); 1 cycle of 1 min mix and 4 min measure (other States).

2.10. Immunofluorescence and laser confocal imaging

Cultured mouse hepatocytes were fixed for 15 min with 4% paraformaldehyde and permeabilized and blocked for 15 min with 0.2% saponin dissolved in 1% BSA-fatty acid free (FAF) in PBS commercial buffer. Tom20 (Santa Cruz) primary antibody was incubated overnight in BSA 1% followed by a secondary antibody for 1 h at room temperature in BSA 0.1%. Filipin (Sigma) was added at 0.33 mg/ml during the secondary antibody incubation and the following steps were performed in the dark. Stained samples were embedded in fluoromount (Sigma) and digital images were taken in a Leica DM2500 confocal microscope.

2.11. Protein carbonylation

Protein carbonylation was assessed by measuring the levels of carbonyl groups using the OxyBlot Protein Oxidation Detection Kit (Millipore), following manufacturer's instruction. The DNPH derivatization was carried out on 10 µg of protein for 15 min. One-dimensional electrophoresis was carried out after DNPH derivatization using 4–12% SDS-polyacrylamide gels (SDS-PAGE) (Bio-Rad, XT-Criterion). Proteins were transferred to nitrocellulose membranes (Bio Rad) which were then blocked with 1% BSA in TBS-Tween. Membranes were then incubated in the primary antibody solution (anti-DNP 1:150) followed by incubation with secondary antibody solution (1:300), both incubations during 1 h at room temperature. After every step, membranes were thoroughly washed with TBS-Tween. Immunoreactive bands were visualized by Pierce ECL Western Blotting Substrate (Thermo Scientific) and band signal intensity was quantified by ImageJ software.

2.12. Statistical analyses

Statistical analyses were performed using GraphPad Prism 6 (Graphpad Software Inc). Unpaired Student's t-test (two tailed) was performed between two groups and one or two-way ANOVA followed by Tukey's Multiple Comparison test were used for statistical comparisons between three or more groups. The corresponding number of experiments is indicated in the figure legends. Data in graphs are shown as mean ± s.e.m.

3. Results

3.1. HC diet alters hepatic cholesterol homeostasis while sodium cholate feeding represses bile acid synthesis

Although feeding a HC diet supplemented with sodium cholate has been previously used as a nutritional approach to steadily increase liver cholesterol content [19,34], the contribution of sodium cholate in the regulation of cholesterol homeostasis in relationship with bile acid synthesis has not been previously examined. Thus, we first

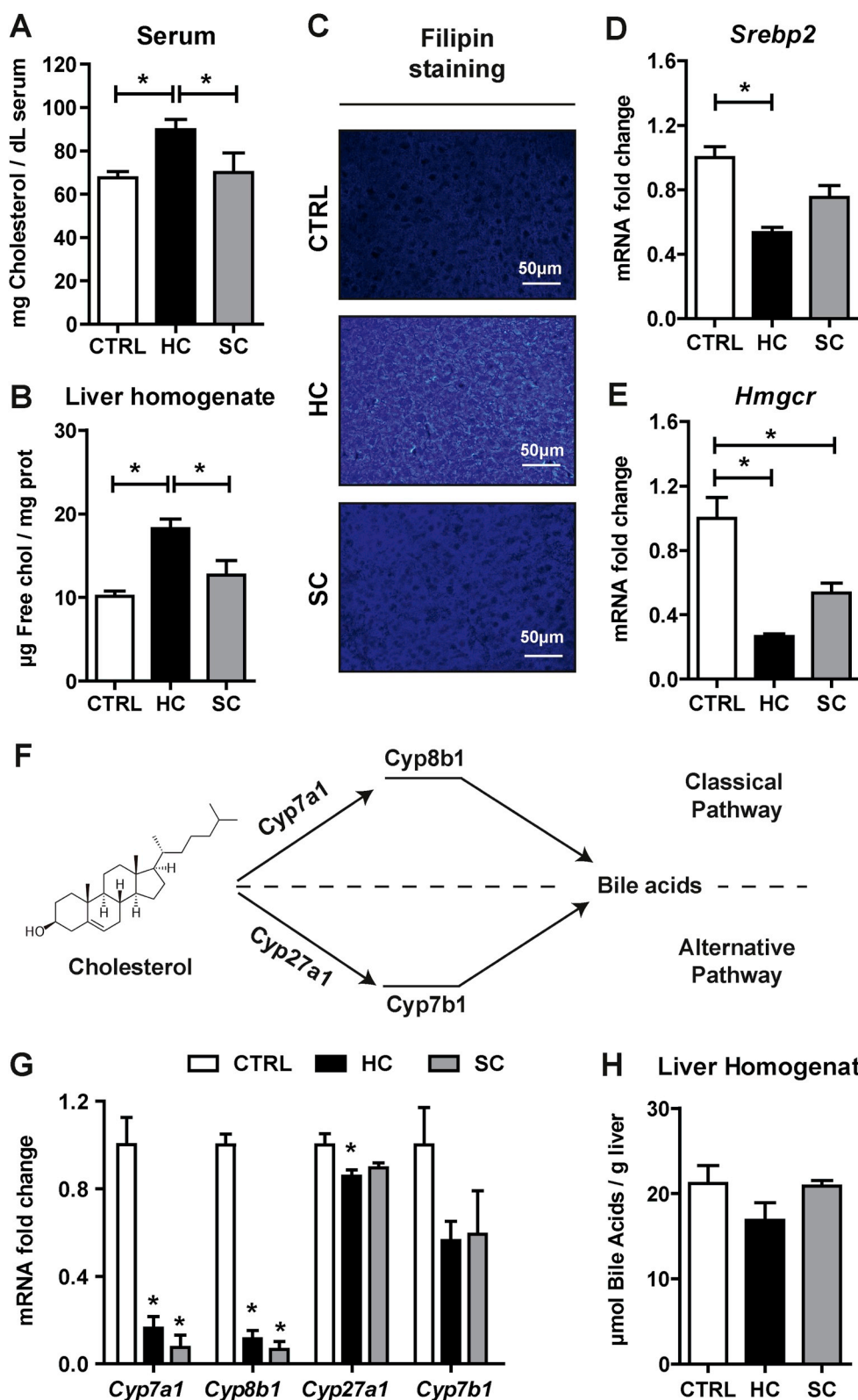


Fig. 1. Alteration of hepatic cholesterol homeostasis and bile acid synthesis by HC feeding. Cholesterol levels in (A) Serum and (B) Liver of WT C57BL/6J mice fed a CTRL, HC or SC (sodium cholate) diet for 2 days. Data are presented as means ± SEM (N > 10, *P < 0.05, One-way ANOVA followed by Tukey's Multiple Comparison test). (C) Cholesterol content in liver by Filipin staining in liver cryosections. Representative images obtained by fluorescence microscopy. (D–E) mRNA levels of *Srebp2* and *Hmgcr* in liver. Values are the mean ± SEM of > 10 animals per group. *P < 0.05. (F) Diagram of classical and alternative pathways of bile acid synthesis in liver. (G) mRNA levels of *Cyp7a1*, *Cyp8b1*, *Cyp27a1* and *Cyp7b1* in liver. Values are the mean ± SEM of > 10 animals per group. *P < 0.05 vs. CTRL samples. (H) Bile Acids levels in liver. Data are presented as means ± SEM (N > 5, *P < 0.05, One-way ANOVA followed by Tukey's Multiple Comparison test).

characterized the regulation of hepatic cholesterol homeostasis and whether dietary cholesterol feeding in the presence of sodium cholate was channeled for bile acids generation. Short-term HC feeding increased cholesterol levels in serum (Fig. 1A) and liver, as determined by HPLC analyses (Fig. 1B), or upon staining of liver sections with filipin to detect free cholesterol levels (Fig. 1C). However, feeding sodium cholate (0.5%) for two days did not significantly increase serum or liver

cholesterol levels (Fig. 1A–C). Moreover, the increase of liver cholesterol levels following HC feeding translated in decreased expression of key steps involved in *de novo* cholesterol biosynthesis, such as *Srebp2* (Fig. 1D), a transcription factor that regulates cholesterol neosynthesis, and its target gene *Hmgcr* (Fig. 1E), which catalyzes the rate-limiting step in the mevalonate pathway. Moreover, as cholesterol is a precursor for bile acids synthesis, we next examined the expression of enzymes

involved in classical (Cyp7a1, Cyp8b1) and the alternative pathway of bile acid synthesis in mitochondria (Cyp27a1, Cyp7b1) (Fig. 1F). While HC feeding markedly decreased the expression of *cyp7a1* as well as *cyp8b1*, this effect was primarily due to the presence of sodium cholate in the diet (Fig. 1G). HC or sodium cholate feeding, however, exerted a modest effect in the expression of Cyp27a1 and Cyp7b1, indicating a minor impact in the alternate pathway of mitochondrial bile acid synthesis. Consistent with these findings, HC feeding did not stimulate the net increase in the total bile acid pool in the liver, likely reflecting the repression by sodium cholate of the enzymes involved in bile acid synthesis (Fig. 1H). Thus, these findings indicate that the presence of sodium cholate in the HC diet contributes to the maintenance of free cholesterol levels, in part, by suppressing its metabolism into bile acid.

3.2. HC-induced mitochondrial cholesterol loading distributes in both mitochondrial membranes and disrupts mitochondrial morphology

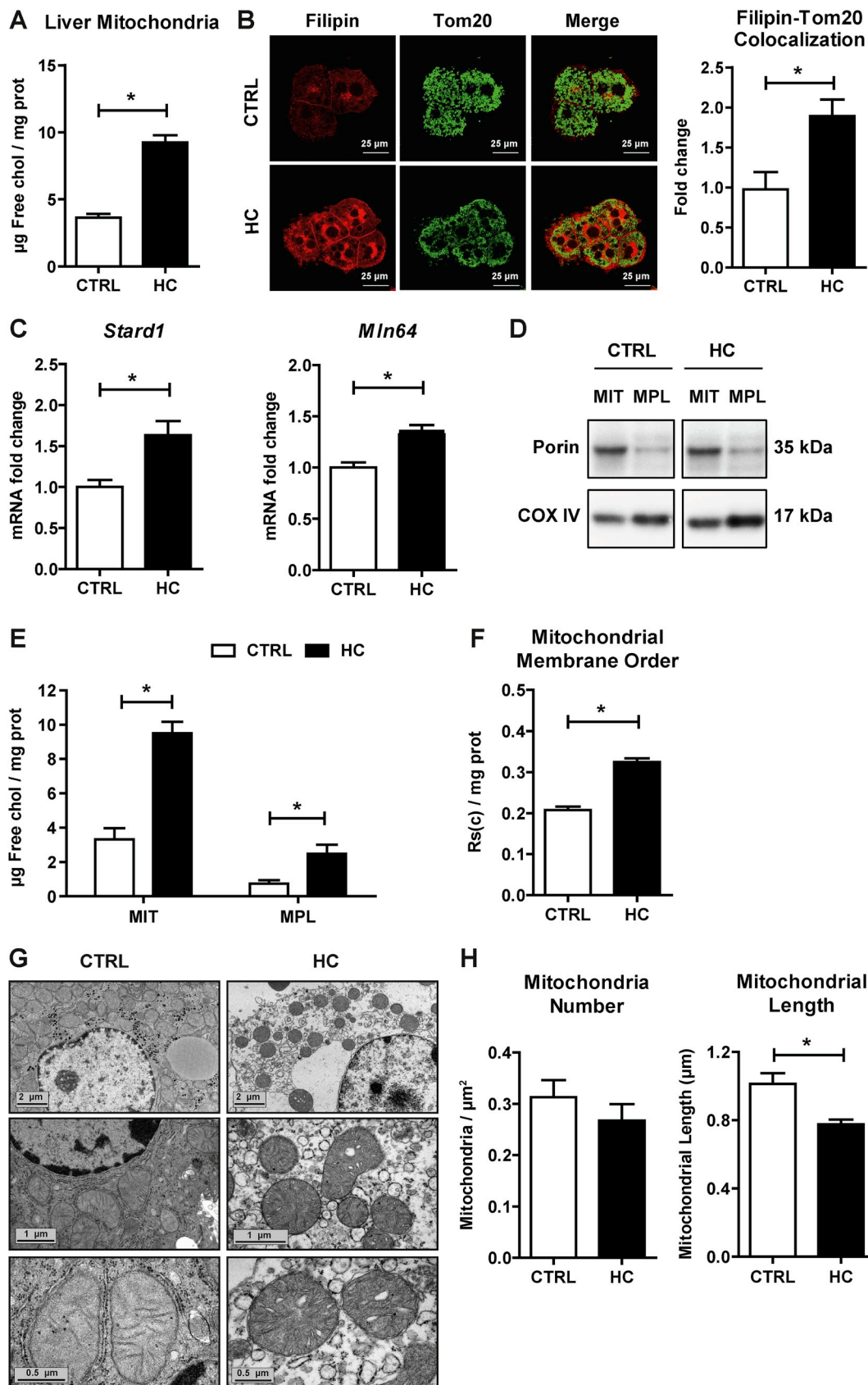
Since HC feeding has been shown to increase mitochondrial cholesterol content [19,34], we next examined the expression of putative mitochondrial cholesterol carriers and the distribution of cholesterol between the outer and inner mitochondrial membranes. Confirming previous findings in rat liver mitochondria [19], isolated mitochondria from HC-fed mice exhibited a significant increase in free cholesterol levels (> 2-fold) determined by HPLC analyses compared to mitochondria from control mice (Fig. 2A). Feeding a 0.5% sodium cholate without cholesterol failed to significantly increase mitochondrial cholesterol levels ($5.7 \pm 0.7 \mu\text{g}$ free cholesterol/mg protein). The increase in mitochondrial cholesterol was also observed by confocal imaging of primary mouse hepatocytes (PMH) isolated from HC-fed mice upon staining with filipin (free-cholesterol marker) and Tom20 (mitochondrial marker). As seen, HC feeding resulted in increased filipin staining, which co-localized with Tom20 indicating increased trafficking of free cholesterol into mitochondria (Fig. 2B). Since STARD1 and MLN64 are known to regulate mitochondrial cholesterol trafficking [14–16,40], we examined their expression in mice fed the HC diet. As shown, *Stard1* and *Mln64* expression increased after HC feeding (Fig. 2C). We next assessed the relative distribution of cholesterol enrichment within mitochondrial membranes. Mitoplasts were isolated from intact mitochondria after permeabilization of the outer membrane upon digitonin treatment. Mitoplasts purity was confirmed by the de-enrichment of porin and the increase in COX IV, compared to intact mitochondria, which was enriched in both markers (Fig. 2D). While cholesterol levels in mitoplasts were lower than in intact mitochondria, the cholesterol content of mitoplasts from cholesterol-enriched mitochondria was higher than in mitoplasts from control mitochondria, indicating the enrichment of cholesterol in both outer and inner mitochondrial membranes (Fig. 2E). The increase of cholesterol in mitochondrial membranes is known to change membrane physical properties [3,19,20]. Thus, we next confirmed whether the presence of cholesterol in mitochondrial membrane inserted into the lipid bilayers and altered membrane fluidity. Fluorescence anisotropy analysis of mitochondria labeled with the fluorescent probe DPH revealed an increase in membrane order of mitochondria from HC-fed animals compared to control mice (Fig. 2F). Moreover, we next addressed whether the loss of mitochondrial fluidity by cholesterol enrichment altered mitochondrial morphology. Electron microscopy analyses revealed that mitochondria from HC-fed mice appeared rounded and with abnormal cristae compared to mitochondria from control animals (Fig. 2G). Although mitochondrial number was not altered by cholesterol accumulation, a significant decrease in mitochondrial length was observed (Fig. 2H). These findings indicate that nutritional cholesterol feeding traffics to mitochondria and alters mitochondrial membrane fluidity and morphology.

3.3. Mitochondrial cholesterol enrichment impairs complex I and complex II-driven state 3 respiration

In view of the preceding findings indicating increased cholesterol in mitochondrial membranes, we next examined the impact of this event in mitochondrial respiration, determining real-time oxygen consumption rates (OCR) by a flux analyzer. Using pyruvate and malate as substrates of complex I, mitochondria from HC-fed mice showed a significant reduction in mitochondrial performance and respiratory states compared to mitochondria from mice-fed control diet (Fig. 3A). In particular, HC feeding impaired ADP-stimulated state 3 respiration as well as the FCCP-induced maximal uncoupler-stimulated respiration (state 3u) without significant change in state 4o respiration (Fig. 3B). These alterations were reflected in the respiratory control ratio (RCR) (state 3/state 4o) and uncoupling control ratio (UCR) (state 3u/state 4o), decreasing both in mitochondria from HC-fed mice (Fig. 3C). Similar analysis was performed using succinate plus rotenone to examine respiration through complex II. HC feeding impaired OCR from succinate plus rotenone with decreased state 3 and state 3u (Fig. 4A and B). In addition, HC feeding decreased succinate plus rotenone-driven state 4o respiration (Fig. 4B), which translated in unchanged RCR and UCR ratios (Fig. 4C). Thus, these findings indicate that *in vivo* mitochondrial cholesterol loading significantly impairs mitochondrial complex I and complex II-driven state 3 respiration. Since the protonmotive force generated from coupled respiration determines the mitochondrial membrane potential, we next assessed the impact of mitochondrial cholesterol loading in membrane potential. Incubation of PMH from HC-fed mice stained with TMRM revealed a decrease in mitochondrial membrane potential (Fig. 3D). Overall, these findings demonstrate the deleterious effects of cholesterol enrichment on mitochondrial respiration.

3.4. Cholesterol-lipid interactions contribute to decreased complex I-driven state 3 respiration

To determine whether the impairment of mitochondrial respiration by HC-induced mitochondrial cholesterol loading is a direct consequence of cholesterol enrichment in mitochondrial membranes, we used an *in situ* approach in which cholesterol complexed with BSA (CBSAC) results in the enrichment of cholesterol content in both membranes [32]. Compared to incubation with BSA alone, CBSAC resulted in the increase in cholesterol levels with a 4-fold increase. Real-time OCR driven by pyruvate plus malate revealed that cholesterol did not affect state 3 or state 3u respiration, although it uncoupled mitochondrial respiration as revealed by the increased state 4o respiration (Fig. 5A), which translated in decreased RCR and UCR (Fig. 5B). However, when succinate plus rotenone were used as substrates the enrichment in cholesterol did not affect succinate-driven OCR and hence RCR and UCR remained unchanged (Fig. 5C and D). Since the interaction of cholesterol with membrane proteins is enantioselective but the interaction with membrane lipids is not [41–43], we next enriched mitochondria with enantiomer cholesterol (Ent-CBSAC), the mirror image of natural cholesterol, as an approach to assess the contribution of the interactions between cholesterol with lipids and/or proteins in the disrupting effect of cholesterol in pyruvate and malate-driven respiration. Mitochondria enriched in Ent-CBSAC exhibited an increase in cholesterol levels similar to those found with natural CBSAC (2.5-fold compared to BSA). As CBSAC failed to alter complex II-driven respiration, we tested the role of Ent-CBSAC on complex I-induced OCR. Interestingly, Ent-CBSAC decreased pyruvate and malate-driven state 3 and state 3u respiration, which resulted in lower RCR and UCR (Fig. 5A and B). These *in vitro* findings suggest that cholesterol-lipid interactions could mediate the decrease in complex I-driven state 3 and state 3u respiration.



(caption on next page)

Fig. 2. Effects of HC feeding on liver mitochondrial cholesterol levels, membrane order and morphology. WT C57BL/6J mice were fed a CTRL or HC diet for 2 days. Cholesterol levels in Mitochondria by (A) HPLC and (B) Immunocytochemistry using Tom20 and Filipin. Staining markers colocalization analyzed using ImageJ software. Data are presented as means \pm SEM (N > 10, *P < 0.05, Unpaired Student's t-test (two tailed)). (C) mRNA levels of *Stard1* and *Mln64* in liver. Values are the mean \pm SEM of > 10 animals per group. *P < 0.05. (D) Purity of mitoplasts from CTRL and cholesterol-enriched mitochondria (Mitochondria = MIT, Mitoplast = MPL). (E) Levels of cholesterol in mitochondria and mitoplasts by HPLC. (F) Mitochondrial membrane order measured by DPH fluorescence anisotropy. (G) Electron microscopy analyses of livers from mice fed a CTRL or HC diet for 2 days. Images were acquired with a Gatan Orius digital camera by moving randomly across the EM grid and are representative of 3 replicates per group. (H) Mitochondrial number and length of liver samples quantified from images of ultrathin sections (G) and analyzed using ImageJ software. Data are presented as means \pm SEM (N = 3, *P < 0.05, Unpaired Student's t-test (two tailed)).

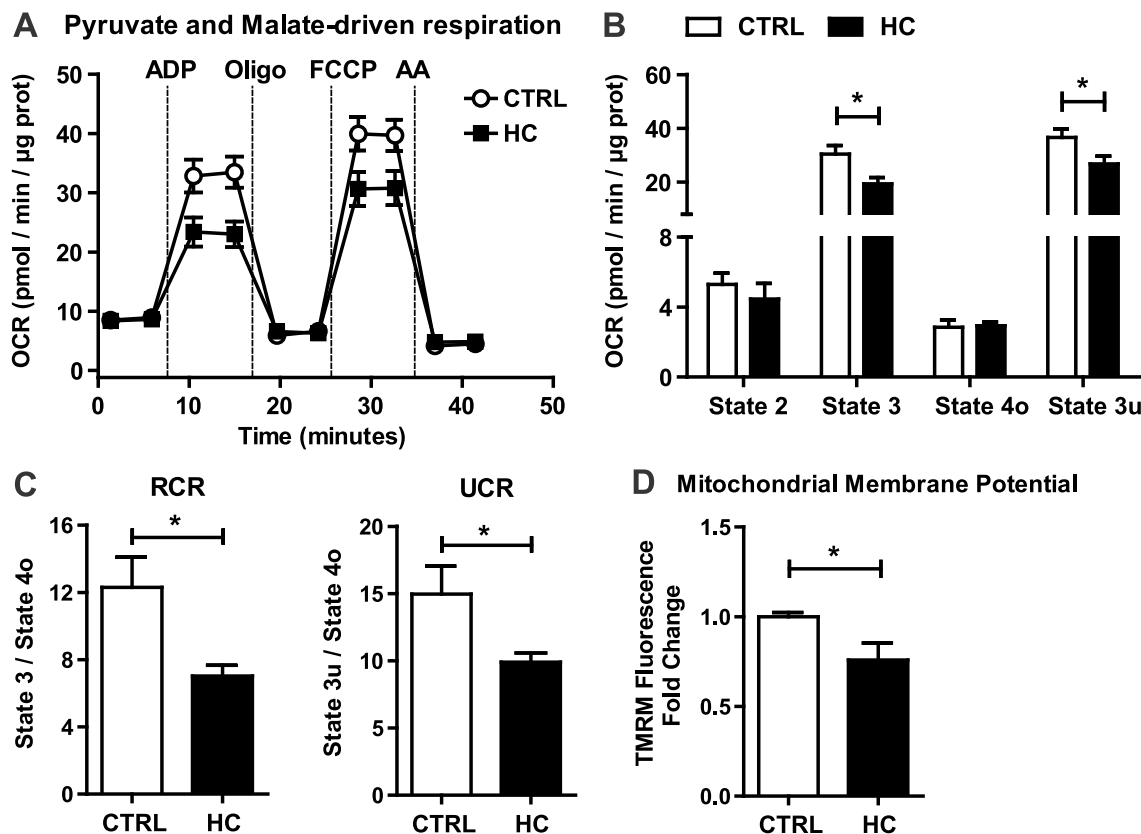


Fig. 3. Effect of cholesterol in mitochondrial OCR using pyruvate and malate as substrates and membrane potential. WT C57BL/6J mice were fed a CTRL or HC diet for 2 days. (A–B) Respiration of CTRL and cholesterol-enriched mitochondria using XFe24 Seahorse Analyzer. Mitochondria began in a coupled state with pyruvate and malate (10 mM) present (state 2). State 3 initiated with ADP (4 mM) addition, state 4 was induced with the injection of oligomycin (2.5 μg/ml) (state 4o), and FCCP (4 μM) induced maximal uncoupler-stimulated respiration (state 3u). Non-mitochondrial respiration was assessed by OCR measurement in the presence of antimycin (4 μM). (C) Respiratory control ratios (RCR: state 3/state 4o, and UCR: state 3u/state 4o). (D) Mitochondrial Membrane Potential measured by TMRM Fluorescence in a fluorescence spectroscopy. Data are presented as means \pm SEM (N = 7 or otherwise stated, *P < 0.05, Unpaired Student's t-test (two tailed)).

3.5. Mitochondrial cholesterol enrichment disrupts the assembly of respiratory supercomplexes

In view of the preceding findings, we hypothesized that mitochondrial cholesterol loading *in vivo* by HC feeding may impact negatively the expression of respiratory complexes. Therefore, we first performed SDS electrophoresis to determine the expression of specific subunits of respiratory complexes. As seen, the expression of specific subunits from complex I (C-I-20), complex II (C-II-30), complex III (C-III-Core 2), complex IV (C-IV-I) and complex V (C-V-α) were unaffected by mitochondrial cholesterol loading by HC feeding (Fig. 6A and B). Since the structural organization of the mitochondrial respiratory complexes as independent entities connected by mobile carriers such as CoQ and cytochrome c has been challenged [39], we next hypothesized that cholesterol-mediated changes in membrane physical properties may

impact the organization and assembly of supercomplexes structures, responsible for carrying out cellular respiration. Blue native electrophoresis of mitochondria after digitonin solubilization was carried out with subsequent antibody incubation against specific subunits of each respiratory complex sequentially. Mitochondrial cholesterol accumulation did not change the levels of respiratory complexes CI, CIV and CV but caused a significant downregulation of respiratory complex III₂ (Fig. 6C and D). This outcome mirrored the downregulation of supercomplexes I₁ + III₂ + IV and I₁ + III₂ in cholesterol-enriched mitochondria (Fig. 6C and D). These data indicating a negative impact of cholesterol on the assembly of respiratory supercomplexes can account for the observed alterations in mitochondrial respiration and emerge as a potential molecular mechanism by which cholesterol accumulation in liver alters mitochondrial function.

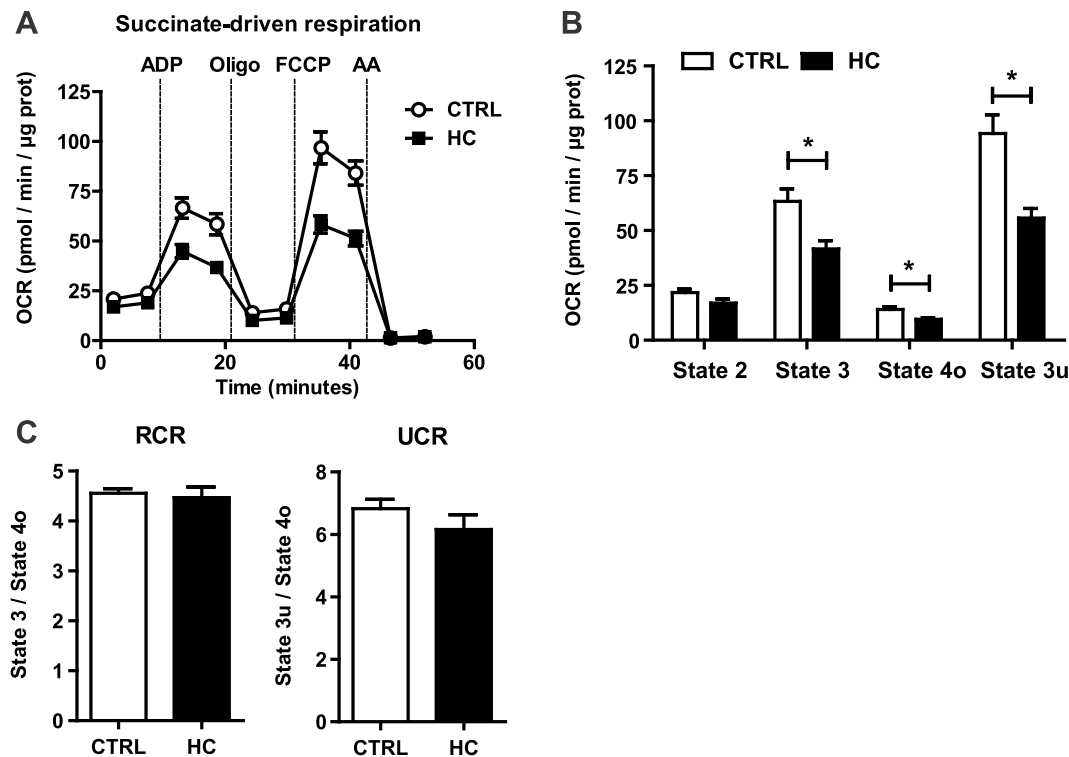


Fig. 4. Effect of cholesterol in mitochondrial respiration from succinate and rotenone. WT C57BL/6J mice were fed a CTRL or HC diet for 2 days. (A–B) Respiration of CTRL and cholesterol-enriched mitochondria using XF24 Seahorse Analyzer. Mitochondria began in a coupled state with succinate (10 mM) and rotenone (2 μM) present (state 2). State 3: ADP (4 mM), State 4o: Oligomycin (2.5 μg/ml), State 3u: FCCP (4 μM), Non-mitochondrial respiration: Antimycin (4 μM). (C) Respiratory control ratios (RCR: state 3/state 4o, and UCR: state 3u/state 4o). Data are presented as means ± SEM (N > 10, *P < 0.05, Unpaired Student's t-test (two tailed)).

3.6. GSH ethyl ester protects against HC-induced oxidative stress and liver injury

As mitochondria are the main consumers of oxygen and a major source of ROS [11–13], we next determined whether HC-induced mitochondrial dysfunction results in increased oxidative stress. As seen, staining of liver sections from HC-fed mice with DHE indicated increased generation of ROS compared to control mice (Fig. 7A and B). This outcome paralleled the depletion of cellular GSH levels (Fig. 7C) as well as the mGSH pool (Fig. 7D), which is primarily due to the defective transport of GSH into mitochondrial matrix [20,29,30]. These findings were accompanied by the stimulation of superoxide anion and especially hydrogen peroxide in isolated mitochondria from HC-fed mice (Supplementary Fig. 1), with the latter effect reflecting the depletion of mGSH induced by mitochondrial cholesterol loading. Consistent with these findings, HC feeding resulted in the increased oxidative stress as shown by enhanced carbonylated proteins (Fig. 7E). HC diet induced a macroscopic change in liver color when compared to control diet. HC livers displayed a steatotic pale appearance compared to control livers (Fig. 7F) that paralleled oil-red staining (Supplementary Fig. 2). In addition, H&E staining revealed a significant dilation of liver perisinusoidal spaces after 2 days of HC feeding (Fig. 7G). These changes were accompanied by the release of AST and ALT in serum indicating that HC-diet induces liver injury (Fig. 7H). We next explored the potential impact of total GSH and mGSH restoration by GSHee in HC-fed mice. GSHee treatment of HC-fed mice restored both total and mGSH pools (Fig. 7C and D). Moreover, GSHee treatment decreased HC-induced DHE increase (Fig. 7A and B), reduced protein carbonylation (Fig. 7E), restored the HC-mediated dilation of liver perisinusoidal

spaces (Fig. 7G), and decreased ALT/AST release, indicating that GSHee protected HC-fed mice from liver injury when compared to HC non-treated mice (Fig. 7H). To assess whether the outcome of GSHee administration was accompanied by improved mitochondrial function, we examined the impact of *in vivo* GSHee administration in mitochondrial performance from pyruvate plus malate-induced OCR. Consistent with previous findings, HC feeding decreased OCR and RCR from complex I that was improved upon GSHee treatment (Fig. 7 I, J). Moreover, GSHee restored the levels of respiratory complex III₂, although it did not affect the assembly of respiratory supercomplexes I + III₂ + IV and I + III₂ (Fig. 7K). Thus, these findings indicate that GSHee administration protects mice from HC-induced liver injury and oxidative stress in part by improving mitochondrial respiration.

4. Discussion

Cholesterol accumulation and, particularly its trafficking to mitochondria, has emerged as a key player in different chronic diseases, including fatty liver disease and hepatocellular carcinoma [12,19,24]. Given the critical structural role of cholesterol in membrane bilayers, the contribution of mitochondrial cholesterol enrichment in disease pathogenesis is exerted in part through its effects in the perturbation of membrane physical properties. However, the specific impact of cholesterol in mitochondrial function and routine performance has not been previously addressed. In order to rapidly increase liver cholesterol levels, we used an *in vivo* approach in which mice were fed a cholesterol-enriched diet supplemented with sodium cholate, which has been shown to sustain liver cholesterol levels [19,34]. Importantly, the presence of sodium cholate in the diet downregulated the expression of

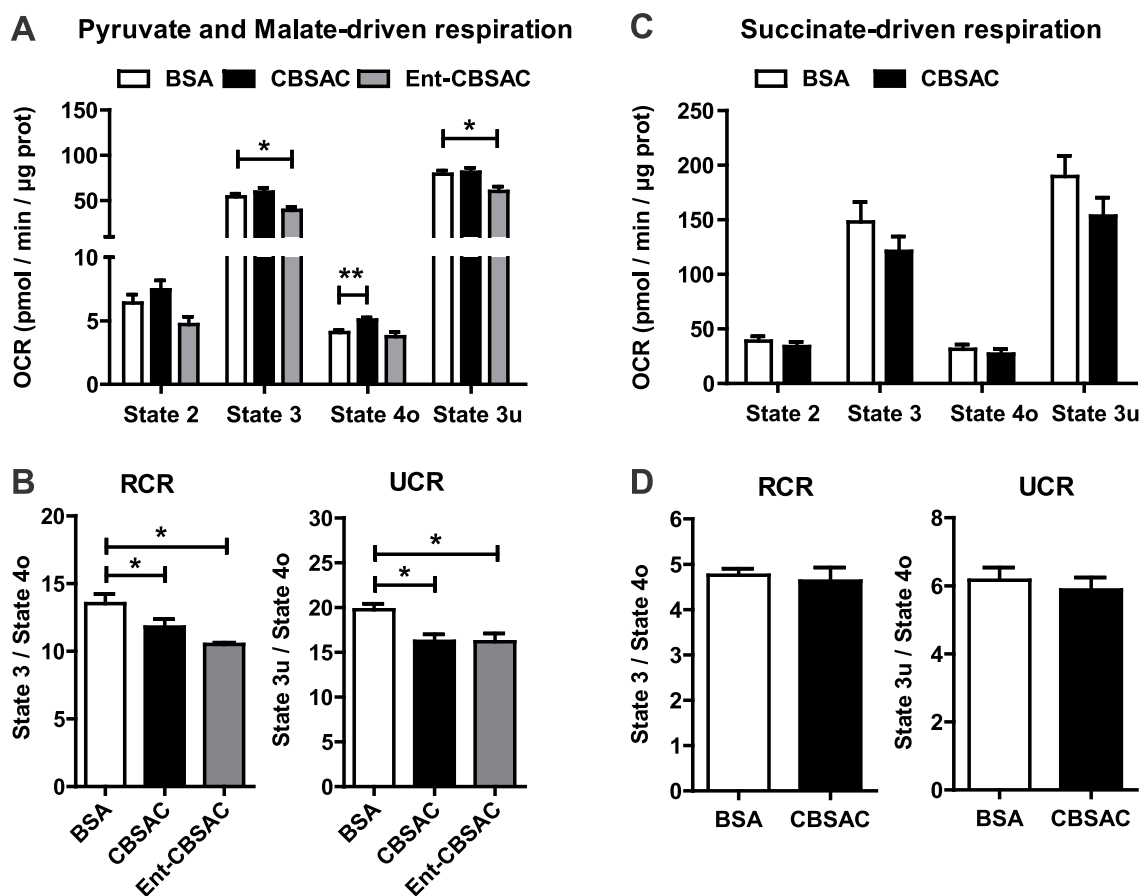


Fig. 5. Impact of *in vitro* cholesterol enrichment in mitochondrial respiration. Mitochondria from WT C57BL/6J mice fed a CTRL diet were isolated and incubated with natural cholesterol or its enantiomer complexed with BSA (CBSAC and Ent-CBSAC respectively). (A) Pyruvate and Malate-driven mitochondrial respiration. State 2: pyruvate and malate (10 mM), State 3: ADP (4 mM), State 4o: Oligomycin (2.5 μ g/ml), State 3u: FCCP (4 μ M), Non-mitochondrial respiration: Antimycin (4 μ M). (B) Respiratory control ratios (RCR: state 3/state 4o, and UCR: state 3u/state 4o). Values are the mean \pm SEM of N > 3 per group. *P < 0.05. One-way ANOVA followed by Tukey's Multiple Comparison test. (C) Succinate and Rotenone-driven mitochondrial respiration. State 2: succinate (10 mM) and rotenone (2 μ M), State 3: ADP (4 mM), State 4o: Oligomycin (2.5 μ g/ml), State 3u: FCCP (4 μ M), Non-mitochondrial respiration: Antimycin (4 μ M). (D) Respiratory control ratios (RCR: state 3/state 4o, and UCR: state 3u/state 4o). Data are presented as means \pm SEM (N > 3, *P < 0.05, Unpaired Student's t-test (two tailed)).

key enzymes involved in the synthesis of bile acids such as Cyp7a1 and Cyp8b1, without effect in the alternate pathway of bile acid synthesis in mitochondria. This finding indicates that sodium cholate is an important component of the HC diet, which contributes to the maintenance of hepatic free cholesterol levels by preventing the metabolism of dietary cholesterol into bile acids.

The *in vivo* loading of hepatic cholesterol levels by HC feeding attenuated the expression of *Srebp2* and *Hmgcr*, which reflects the alterations in endogenous cholesterol homeostasis, an effect that was accompanied by its accumulation in mitochondria. This outcome paralleled the increased expression of *Stard1* and *Mln64*, which play critical roles in the regulation of mitochondrial trafficking [14–16]. Importantly, mitochondrial fractionation into mitoplasts revealed that cholesterol accumulation occurs in both the outer and inner mitochondrial membranes, consistent with a concerted action between MLN64 and STARD1, which move cholesterol from extramitochondrial sources to the outer mitochondrial membrane and from here to the inner mitochondrial membrane, respectively [14–16]. Of relevance, we show that *in vivo* cholesterol accumulation impairs mitochondrial oxidative phosphorylation, reflected in decreased ADP-stimulated OCR from complex I, which translated in decreased RCR and UCR. This outcome is accompanied by the defective assembly of respiratory

supercomplexes I₁ + III₂ + IV and I₁ + III₂. These findings are consistent with the current concept that mitochondrial supercomplexes structures are responsible for carrying out cellular respiration [39,44], as opposed to the long-held view of mitochondrial respiratory complexes as independent entities connected by mobile carriers CoQ and cytochrome c. The vast majority of the subunits of the mitochondrial respiratory complexes are encoded by nuclear DNA, which then traffic to mitochondria by the presence of intramitochondrial sorting signals to undergo a highly-regulated mechanism of import and insertion into mitochondrial membranes [45]. However, hepatic cholesterol loading does not affect the expression of specific subunits of complex I–V, suggesting that the effect of mitochondrial cholesterol in the assembly of the mitochondrial supercomplexes may reflect defects at the mitochondrial membrane level likely due to changes in membrane physical properties. This outcome is consistent with recent findings pointing that membrane lipid composition determines cellular respiration through changes in membrane fluidity and physical properties [46,47]. Indeed, reconstitution of complex I and complex III in proteoliposomes with different lipid composition revealed that the ratio of phospholipid to protein determines the assembly of supercomplex I₁-III₂ [46]. Moreover, studies in bacteria engineered to express increased levels of unsaturated fatty acids unraveled that membrane viscosity

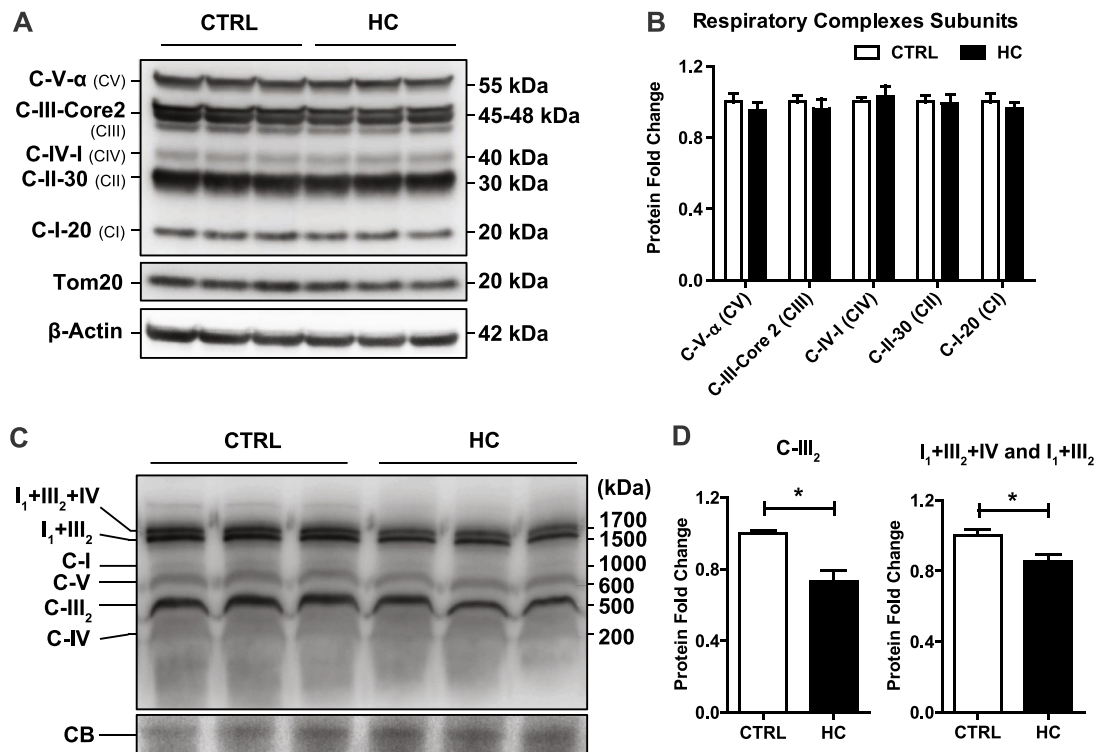


Fig. 6. Impairment of mitochondrial supercomplexes assembly by cholesterol enrichment. (A) Protein expression of mitochondrial respiratory complexes subunits from livers of WT C57BL/6J mice fed a CTRL or HC diet for 2 days. β -Actin was used as loading control. Images are representative of at least three independent experiments. (B) Protein Expression quantification of (A) by ImageJ software. Values are the mean \pm SEM of > 5 animals per group. * $P < 0.05$ vs. CTRL samples. (C) Blue Native Page electrophoresis of livers from CTRL and HC mice to detect OXPHOS complexes and Supercomplexes expression. Coomassie Blue (CB) staining was used as loading control. Images are representatives of 9 replicates per group. (D) Protein Expression quantification of (C) by ImageJ software. Values are the mean \pm SEM of $N > 5$ animals per group. * $P < 0.05$. Unpaired Student's t-test (two tailed).

determined by lipid composition controlled the rate of respiration coupled to ADP phosphorylation [47]. Whether the deleterious effect of cholesterol enrichment in mitochondrial function is reversible upon cholesterol extraction or membrane fluidization remains to be further investigated. In line with this possibility, Yu et al. showed that the defective ATPase function from brain mitochondria from NPC knockout mice, which exhibit an increased mitochondrial cholesterol loading, was restored by cholesterol extraction with cyclodextrin [48]. Thus, while mitochondrial cholesterol loading *in vivo* by feeding the HC diet may reflect the combined effect of cholesterol on established and newly assembled respiratory complexes by membrane mediated changes, we addressed the direct impact of cholesterol enrichment in the existing respiratory complexes in isolated mitochondria and whether this event involves interactions of cholesterol with bilayer's proteins and/or lipids using enantiomer cholesterol, the mirror image of natural cholesterol. Enrichment of liver mitochondria in enantiomer cholesterol, which specifically interacts with lipids but not proteins due to enantioselective restriction [37,41–43], resulted in decreased complex I-driven state 3/state 3u respiration, suggesting that cholesterol-lipid interactions in mitochondrial membranes accounts for the impaired ADP-stimulated OCR driven by complex I. Intriguingly, although *in vitro* cholesterol loading increased complex I-driven state 4o respiration, this outcome was not observed with the *in vivo* mitochondrial cholesterol loading by HC feeding. Whether cholesterol-lipid interactions is a predominant effect over the interaction of cholesterol with proteins to account for the decreased complex I-driven state 3/3u respiration remains to be further investigated. Interestingly, *in situ* cholesterol enrichment in

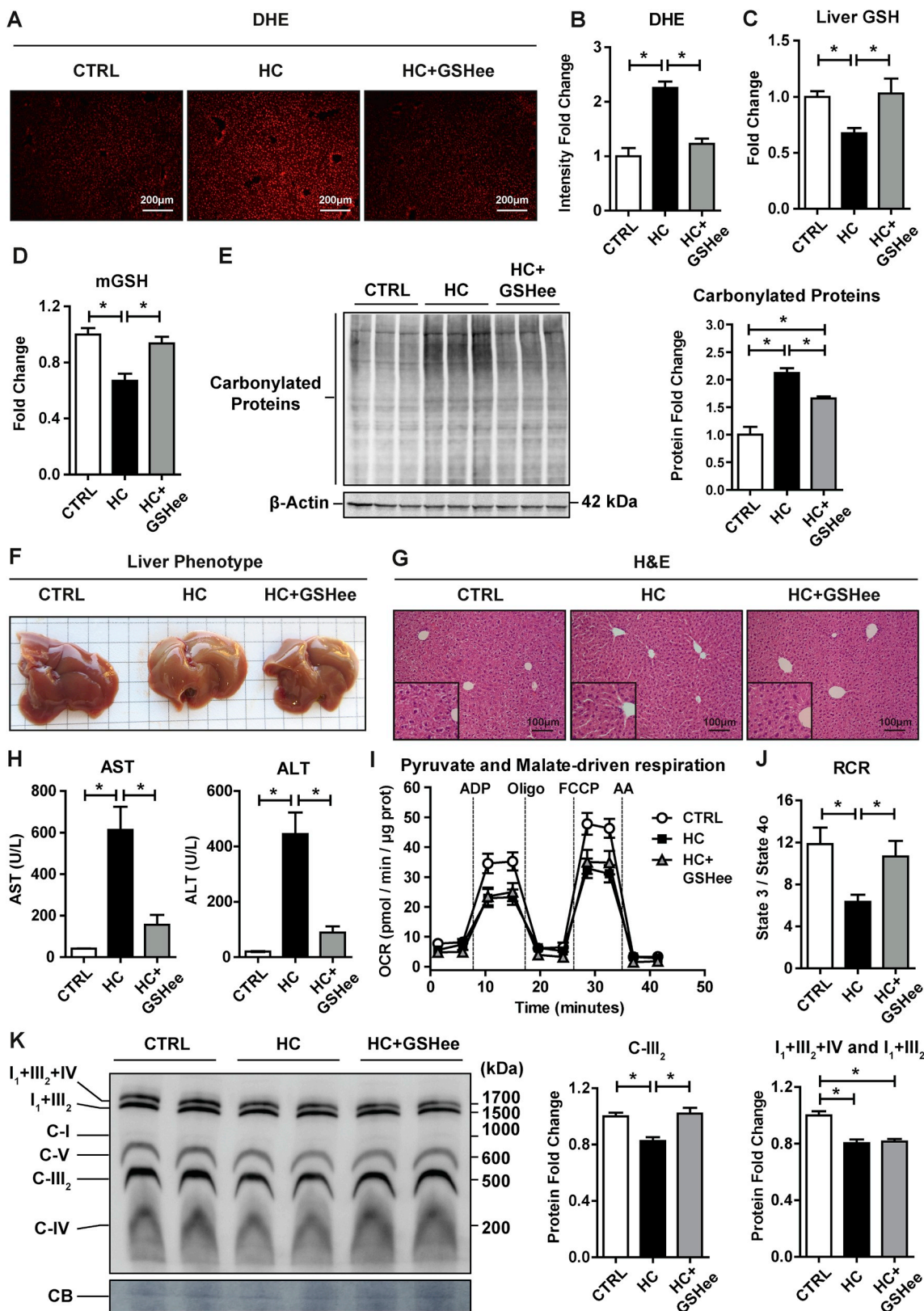
mitochondria did not affect complex II-driven OCR although *in vivo* mitochondrial cholesterol loading did impair state 3 respiration. This differential effect suggests that the impact of cholesterol in impairing complex II-mediated OCR reflects the impact of cholesterol in the assembly of respiratory supercomplexes rather than a direct effect of the changes in membrane physical properties.

A caveat from the *in vivo* enrichment of mitochondria in cholesterol on mitochondrial respiration by feeding a HC enriched diet is whether the effects truly reflect the actions of cholesterol *per se* or are determined by cholesterol-derived metabolites. As cholesterol is the precursor of bile acids, it is conceivable that part of the observed effects of cholesterol enrichment in mitochondrial performance could be mediated by the action of bile acids generated from dietary cholesterol. This potential contribution, however, seems unlikely in light of the fact that the presence of sodium cholate in the HC-enriched diet impaired the classical pathway of bile acid synthesis due to decreased the expression of *cyp7a1* and *cyp8b1*, consistent with the lack of increased bile acid pool from HC-fed mice.

As one of the reported consequences of the disruption of the association between complex I and complex III and the impaired assembly of subsequent supercomplexes I₁+III₂+IV and I₁+III₂ is the enhanced generation of superoxide anion [46], we analyzed the impact of mitochondrial cholesterol enrichment in oxidative stress and liver injury. While HC feeding caused increased ROS formation, mitochondrial ROS generation and mGSH depletion that was accompanied by steatosis and liver injury, these events were recovered by GSHee administration. Interestingly, the effect of mGSH restoration by GSHee translated in

replenishing mitochondrial respiration and RCR, in line with previous findings in cerebellar mitochondrial function in NPC disease [35]. Restoration of mGSH levels by GSHee rescued the content of complex III₂, although it failed to normalize the assembly of supercomplexes I + III₂ + IV and I + III₂, which likely reflects the effect of remaining

cholesterol-mediated effect on membrane dynamics that are not reversed by mGSH restoration. However, quite intriguingly, the restoration of complex III₂ by GSHee seems to compensate the function of mitochondrial respiration. Further work will be required to determine the mechanisms whereby mGSH depletion by mitochondrial cholesterol



(caption on next page)

Fig. 7. Effects of GSHee treatment on HC-induced oxidative stress and liver damage. (A) Reactive oxygen species content in liver tissue by DHE staining. Representative images obtained by fluorescence microscopy. (B) Fluorescence quantification of DHE intensity using ImageJ software. (C–D) GSH levels in liver and mitochondria. Values are the mean \pm SEM of > 5 animals per group. * P < 0.05. One-way ANOVA followed by Tukey's Multiple Comparison test. (E) Carbonylated proteins from liver sections of CTRL or HC-fed mice with or without GSHee administration *in vivo*. Results are the mean \pm SEM of 3 animals per group. * P < 0.05. One-way ANOVA followed by Tukey's Multiple Comparison test. (F) Macroscopic view of liver after CTRL or HC feeding with or without GSHee treatment. Representative image of > 5 replicates is shown. (G) Liver sections of CTRL, HC and HC + GSHee mice analyzed by H&E. (H) Serum AST and ALT levels from CTRL, HC and HC + GSHee mice. Data are presented as means \pm SEM (N > 5, * P < 0.05, One-way ANOVA followed by Tukey's Multiple Comparison test). (I) Pyruvate and Malate-driven mitochondrial respiration. State 2: pyruvate and malate (10 mM), State 3: ADP (4 mM), State 4o: Oligomycin (2.5 μ g/ml), State 3u: FCCP (4 μ M), Non-mitochondrial respiration: Antimycin (4 μ M). (J) Respiratory control ratio (RCR: state 3/state 4o) determined from OCR analyzed in I. (K) Blue Native Page electrophoresis of livers from CTRL and HC-fed mice with or without GSHee treatment to detect OXPHOS complexes and Supercomplexes expression. Coomassie Blue (CB) staining was used as loading control. Results are the mean \pm SEM of 8 animals per group. * P < 0.05. One-way ANOVA followed by Tukey's Multiple Comparison test. (For interpretation of the references to color in this figure legend, the reader is referred to the Web version of this article.)

loading impact the redox-dependent assembly of supercomplexes assembly and whether the reversible loss of complex III₂ by cholesterol is redox dependent in view of its restoration by mGSH with GSHee.

Acknowledgments

We want to thank Dr. José A. Enriquez and Sara Cogliati from the CNIC, Madrid, Spain for valuable suggestions and comments regarding the supercomplexes analysis. We want to acknowledge the Electronic microscopy (TEM/SEM) facility of the University of Barcelona (CCiT-UB) for the electron microscopy studies. We acknowledge the support from grants SAF2014-57674R, SAF-2015-69944R, and SAF2017-85877R from Plan Nacional de I+D, by the CIBEREHD from the Instituto de Salud Carlos III, by AGAUR of the Generalitat de Catalunya SGR-2017-1112, and by the Fundación BBVA, Spain. We also acknowledge support from the center grant P50AA011999 Southern California Research Center for ALPD and Cirrhosis funded by NIAAA/NIH and by the European Cooperation in Science and Technology (COST) ACTION CA17112 Prospective European Drug-Induced Liver Injury Network. We also acknowledge the gift of enantiomer cholesterol by Dr. Scott Rychnovsky (Department of Chemistry, University of California Irvine).

E.S.-V. was supported by a contract from the “Ministerio de Educación, Cultura y Deporte” (FPU15/04537) of the Spanish Government. R.F. was funded by “Juan de la Cierva Incorporación” from the National Programme for the Promotion of Talent and Its Employability of the “Ministerio de Ciencia, Innovación y Universidades” (IJCI-2015-23219) of the Spanish Government. Mitochondria and protein images from graphical abstract were taken and adapted from Smart Servier Medical Art under Creative Commons Attribution 3.0 Unported License.

Appendix A. Supplementary data

Supplementary data to this article can be found online at <https://doi.org/10.1016/j.redox.2019.101214>.

References

- G. Gimpl, K. Burger, F. Fahrenholz, Cholesterol as modulator of receptor function, *Biochemistry* 36 (1997) 10959–10974.
- K. Simons, R. Ehehalt, Cholesterol, lipid rafts, and disease, *J. Clin. Investig.* 110 (2002) 597–603.
- F.R. Maxfield, I. Tabas, Role of cholesterol and lipid organization in disease, *Nature* 438 (2005) 612–621.
- J.D. Horton, J.L. Goldstein, M.S. Brown, SREBPs: activators of the complete program of cholesterol and fatty acid synthesis in the liver, *J. Clin. Investig.* 109 (2002) 1125–1131.
- S.W. Tait, D.R. Green, Mitochondria and cell signalling, *J. Cell Sci.* 125 (Pt 4) (2012) 807–815.
- J. Nunnari, A. Suomalainen, Mitochondria: in sickness and in health, *Cell* 148 (6) (2012 Mar 16) 1145–1159.
- B. Westermann, Mitochondrial fusion and fission in cell life and death, *Nat. Rev. Mol. Cell Biol.* 11 (12) (2010 Dec) 872–884.
- P. Mishra, D.C. Chan, Mitochondrial dynamics and inheritance during cell division, development and disease, *Nat. Rev. Mol. Cell Biol.* 15 (10) (2014 Oct) 634–646.
- T. Wai, T. Langer, Mitochondrial dynamics and metabolic regulation, *Trends Endocrinol. Metabol.* 27 (2) (2016 Feb) 105–117.
- A. Murley, J. Nunnari, The emerging network of mitochondria-organelle contacts, *Mol. Cell* 61 (5) (2016 Mar 3) 648–653.
- M.P. Murphy, Understanding and preventing mitochondrial oxidative damage, *Biochem. Soc. Trans.* 44 (5) (2016 Oct 15) 1219–1226.
- C. Garcia Ruiz, J.C. Fernandez-Checa, Mitochondrial oxidative stress and anti-oxidants balance in fatty liver disease, *Hepatol. Commun.* (2) (2018 Oct 30) 1425–1439.
- T. Finkel, Signal transduction by mitochondrial oxidants, *J. Biol. Chem.* 287 (7) (2012 Feb 10) 4434–4440.
- W.L. Miller, Steroidogenic acute regulatory protein (StAR), a novel mitochondrial cholesterol transporter, *Biochim. Biophys. Acta* 1771 (6) (2007 Jun) 663–676.
- K.M. Caron, S.C. Soo, W.C. Wetzel, D.M. Stocco, B.J. Clark, K.L. Parker, Targeted disruption of the mouse gene encoding steroidogenic acute regulatory protein provides insights into congenital lipid adrenal hyperplasia, *Proc. Natl. Acad. Sci. U. S. A.* 94 (21) (1997 Oct 14) 11540–11545.
- P. Elustondo, L.A. Martin, B. Karten, Mitochondrial cholesterol import, *Biochim. Biophys. Acta Mol. Cell Biol. Lipids* 1862 (1) (2017 Jan) 90–101.
- G. van Meer, D.R. Voelker, G.W. Feigenson, Membrane lipids: where they are and how they behave, *Nat. Rev. Mol. Cell Biol.* 9 (2008) 112–124.
- A. Baulies, J. Montero, N. Matías, N. Insausti, O. Terrones, G. Basañez, C. Vallejo, L. Conde de La Rosa, L. Martinez, D. Robles, A. Morales, J. Abian, M. Carrascal, K. Machida, D.B.U. Kumar, H. Tsukamoto, N. Kaplowitz, C. Garcia-Ruiz, J.C. Fernández-Checa, The 2-oxoglutarate carrier promotes liver cancer by sustaining mitochondrial GSH despite cholesterol loading, *Redox Biol.* 14 (2018 Apr) 164–177.
- M. Marí, F. Caballero, A. Colell, A. Morales, J. Caballeria, A. Fernandez, C. Enrich, J.C. Fernandez-Checa, C. Garcia-Ruiz, Mitochondrial free cholesterol loading sensitizes to TNF- and Fas-mediated steatohepatitis, *Cell Metabol.* 4 (3) (2006 Sep) 185–198.
- A. Fernández, A. Colell, F. Caballero, N. Matías, C. García-Ruiz, J.C. Fernández-Checa, Mitochondrial S-adenosyl-L-methionine transport is insensitive to alcohol-mediated changes in membrane dynamics, *Alcohol Clin. Exp. Res.* 33 (7) (2009 Jul) 1169–1180.
- L.G. Baggetto, R. Testa-Parussini, Role of acetoin on the regulation of intermediate metabolism of Ehrlich ascites tumor mitochondria: its contribution to membrane cholesterol enrichment modifying passive proton permeability, *Arch. Biochem. Biophys.* 283 (1990) 241–248.
- L.G. Baggetto, E. Clottes, C. Vial, Low mitochondrial proton leak due to high membrane cholesterol content and cytosolic creatine kinase as two features of the deviant bioenergetics of Ehrlich and AS30-D tumor cells, *Cancer Res.* 52 (1992) 4935–4941.
- S.W. Ballinger, Mitochondrial dysfunction in cardiovascular disease, *Free Radic. Biol. Med.* 38 (2005) 1278–1295.
- V. Ribas, C. García-Ruiz, J.C. Fernández-Checa, Mitochondria, cholesterol and cancer cell metabolism, *Clin. Transl. Med.* 5 (1) (2016 Dec) 22.
- J. Montero, A. Morales, L. Llacuna, J.M. Lluís, O. Terrones, G. Basañez, B. Antonsson, J. Prieto, C. García-Ruiz, A. Colell, J.C. Fernández-Checa, Mitochondrial cholesterol contributes to chemotherapy resistance in hepatocellular carcinoma, *Cancer Res.* 68 (13) (2008) 5246–5256.
- A. Fernández, L. Llacuna, J.C. Fernandez-Checa, A. Colell, Mitochondrial cholesterol loading exacerbates amyloid beta peptide-induced inflammation and neurotoxicity, *J. Neurosci.* 29 (20) (2009) 6394–6405.
- F. Feo, R.A. Canuto, R. Garcea, L. Gabriel, Effect of cholesterol content on some physical and functional properties of mitochondria isolated from adult rat liver, fetal liver, cholesterol-enriched liver and hepatomas AH-130, 3924A and 5123, *Biochim. Biophys. Acta* 413 (1975) 116–134.
- R.C. Crain, R.W. Clark, B.E. Harvey, Role of lipid transfer proteins in the abnormal lipid content of Morris hepatoma mitochondria and microsomes, *Cancer Res.* 43 (1983) 3197–3202.
- C. Garcia-Ruiz, A. Morales, A. Ballesta, J. Rodes, N. Kaplowitz, J.C. Fernandez-Checa, Effect of chronic ethanol feeding on glutathione and functional integrity of mitochondria in periportal and perivenous rat hepatocytes, *J. Clin. Investig.* 94 (1994) 193–201.
- A. Colell, C. Garcia-Ruiz, A. Morales, et al., Transport of reduced glutathione in hepatic mitochondria and mitoplasts from ethanol-treated rats: effect of membrane physical properties and S-adenosyl-L-methionine, *Hepatology* 26 (1997) 699–708.
- O. Coll, A. Colell, C. Garcia-Ruiz, N. Kaplowitz, J.C. Fernandez-Checa, Sensitivity of the 2-oxoglutarate carrier to alcohol intake contributes to mitochondrial

- glutathione depletion, *Hepatology* 38 (2003) 692–702.
- [32] A. Colell, C. Garcia-Ruiz, J.M. Lluís, O. Coll, M. Marí, J.C. Fernandez-Checa, Cholesterol impairs the adenine nucleotide translocator-mediated mitochondrial permeability transition through altered membrane fluidity, *J. Biol. Chem.* 278 (2003) 33928–33935.
- [33] Shuang Mei, Haihua Gu, Xuefeng Yang, Huailan Guo, Zhenqi Liu, Wenhong Cao, Prolonged exposure to insulin induces mitochondrion-derived oxidative stress through increasing mitochondrial cholesterol content in hepatocytes, *Endocrinology* 153 (5) (2012) 2120–2129.
- [34] M. Domínguez-Pérez, A. Simoni-Nieves, P. Rosales, N. Nuño-Lámbardi, M. Rosas-Lemus, V. Souza, R.U. Miranda, L. Bucio, S. Uribe Carvajal, J.U. Marquardt, D. Seo, L.E. Gomez-Quiroz, M.C. Gutiérrez-Ruiz, Cholesterol burden in the liver induces mitochondrial dynamic changes and resistance to apoptosis, *J. Cell. Physiol.* 234 (2019 May) 7213–7223.
- [35] S. Torres, N. Matías, A. Baulies, S. Nuñez, C. Alarcon-Vila, L. Martinez, N. Nuño, A. Fernandez, J. Caballeria, T. Levade, A. Gonzalez-Franquesa, P. Garcia-Rovés, E. Balboa, S. Zanlungo, G. Fabrias, J. Casas, C. Enrich, C. Garcia-Ruiz, J.C. Fernández-Checa, Mitochondrial GSH replenishment as a potential therapeutic approach for Niemann Pick type C disease, *Redox Biol.* 11 (2017 Apr) 60–72.
- [36] C. Von Montfort, N. Matias, A. Fernandez, R. Fucho, L. Conde de la Rosa, M.L. Martinez-Chantar, J.M. Mato, K. Machida, H. Tsukamoto, M.P. Murphy, A. Mansouri, N. Kaplowitz, C. Garcia-Ruiz, J.C. Fernandez-Checa, Mitochondrial GSH determines the toxic or therapeutic potential of superoxide scavenging in steatohepatitis, *J. Hepatol.* 57 (2012) 852–859.
- [37] I. Kristiana, W. Luu, J. Stevenson, S. Cartland, W. Jessup, J.D. Belani, S.D. Rychnovsky, A.J. Brown, Cholesterol through the looking glass: ability of its enantiomer also to elicit homeostatic responses, *J. Biol. Chem.* 287 (40) (2012 Sep 28) 33897–33904.
- [38] I. Wittig, H.P. Braun, H. Schägger, Blue native page, *Nat. Protoc.* 1 (1) (2006) 418–428.
- [39] R. Acín-Pérez, P. Fernández-Silva, M.L. Peleato, A. Pérez-Martos, J.A. Enriquez, Respiratory active mitochondrial supercomplexes, *Mol. Cell* 32 (4) (2008 Nov 21) 529–539.
- [40] E. Balboa, J. Castro, M.J. Pinochet, G.I. Cancino, N. Matías, P. José Sáez, A. Martínez, A.R. Álvarez, C. Garcia-Ruiz, J.C. Fernandez-Checa, S. Zanlungo, MLN64 induces mitochondrial dysfunction associated with increased mitochondrial cholesterol content, *Redox Biol.* 12 (2017 Aug) 274–284.
- [41] F. Xu, S.D. Rychnovsky, J.D. Belani, H.H. Hobbs, J.C. Cohen, R.B. Rawson, Dual roles for cholesterol in mammalian cells, *Proc. Natl. Acad. Sci. U. S. A.* 102 (41) (2005 Oct 11) 14551–14556.
- [42] E.J. Westover, D.F. Covey, The enantiomer of cholesterol, *J. Membr. Biol.* 202 (2) (2004 Nov) 61–72.
- [43] Y. Li, M. Ge, L. Ciani, G. Kuriakose, E.J. Westover, M. Dura, D.F. Covey, J.H. Freed, F.R. Maxfield, J. Lytton, I. Tabas, Enrichment of endoplasmic reticulum with cholesterol inhibits sarcoplasmic-endoplasmic reticulum calcium ATPase-2b activity in parallel with increased order of membrane lipids: implications for depletion of endoplasmic reticulum calcium stores and apoptosis in cholesterol-loaded macrophages, *J. Biol. Chem.* 279 (35) (2004 Aug 27) 37030–37039.
- [44] R. Acín-Pérez, J.A. Enriquez, The function of the respiratory supercomplexes: the plasticity model, *Biochim. Biophys. Acta* 1837 (4) (2014 Apr) 444–450.
- [45] S.E. Horvath, H. Rampelt, S. Oeljeklaus, B. Warscheid, M. van der Laan, N. Pfanner, Role of membrane contact sites in protein import into mitochondria, *Protein Sci.* 24 (3) (2015 Mar) 277–297.
- [46] E. Maranzana, G. Barbero, A.I. Falasca, G. Lenaz, M.L. Genova, Mitochondrial respiratory supercomplex association limits production of reactive oxygen species from complex I, *Antioxidants Redox Signal.* 119 (2013) 1469–1480.
- [47] I. Budin, R. de Rond, Y. Chen, L.J. Chan, C.J. Petzold, J.D. Keasling, Viscous control of cellular respiration by membrane lipid composition, *Science* 326 (2018 Dec 7) 1186–1189.
- [48] W. Yu, J.S. Gong, M. Ko, W.S. Garver, K. Yanagisawa, M. Michikawa, Altered cholesterol metabolism in Niemann-Pick type C1 mouse brains affects mitochondrial function, *J. Biol. Chem.* 280 (12) (2005 Mar 25) 11731–11739.